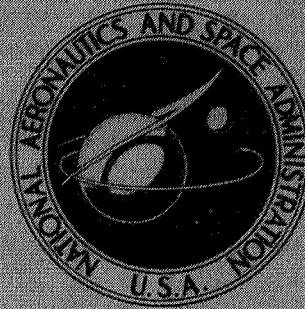


N71-22681

NASA TECHNICAL
MEMORANDUM



NASA TM X-2238

NASA TM X-2238

CASE FILE
COPY

EXPERIMENTAL INVESTIGATION
OF TWO METHODS FOR GENERATING
AN ARTIFICIALLY THICKENED
BOUNDARY LAYER

by David F. Johnson and Glenn A. Mitchell

Lewis Research Center

Cleveland, Ohio 44135

NATIONAL AERONAUTICS AND SPACE ADMINISTRATION • WASHINGTON, D. C. • APRIL 1971

1. Report No. NASA TM X-2238	2. Government Accession No.	3. Recipient's Catalog No.	
4. Title and Subtitle EXPERIMENTAL INVESTIGATION OF TWO METHODS FOR GENERATING AN ARTIFICIALLY THICKENED BOUNDARY LAYER		5. Report Date April 1971	6. Performing Organization Code
		8. Performing Organization Report No. E-5997	10. Work Unit No. 720-03
7. Author(s) David F. Johnson and Glenn A. Mitchell		11. Contract or Grant No.	
9. Performing Organization Name and Address Lewis Research Center National Aeronautics and Space Administration Cleveland, Ohio 44135		13. Type of Report and Period Covered Technical Memorandum	
		14. Sponsoring Agency Code	
12. Sponsoring Agency Name and Address National Aeronautics and Space Administration Washington, D.C. 20546		15. Supplementary Notes	
16. Abstract A study has been made of techniques for generating an artificially thickened boundary layer on a flat plate. The boundary-layer generation was accomplished by means of locating protuberances on the leading-edge surface of the plate. Two protuberance designs were investigated: cylindrical and biconical. The investigation was conducted at Mach numbers 2.3 to 2.6 and at a Reynolds number of 2.4×10^6 per foot ($7.87 \times 10^6/m$). The results of the investigation revealed that both protuberances were effective in thickening the boundary layer. However, the conical protuberances produced thicker boundary layers with less flow distortions.			
17. Key Words (Suggested by Author(s)) Turbulent boundary layer		18. Distribution Statement Unclassified - unlimited	
19. Security Classif. (of this report) Unclassified	20. Security Classif. (of this page) Unclassified	21. No. of Pages 38	22. Price* \$3.00

* For sale by the National Technical Information Service, Springfield, Virginia 22151

EXPERIMENTAL INVESTIGATION OF TWO METHODS FOR GENERATING AN ARTIFICIALLY THICKENED BOUNDARY LAYER

by David F. Johnson and Glenn A. Mitchell

Lewis Research Center

SUMMARY

A study has been made of techniques for generating an artificially thickened boundary layer on a flat plate for wind tunnel investigations. The boundary-layer generation was accomplished by means of locating protuberances on the leading-edge surface of the flat plate. Two configurations of protuberances, cylindrical protuberances and biconical protuberances, were investigated.

The investigation was conducted in a Mach number range of 2.3 to 2.6 with a free-stream Reynolds number of 2.4×10^6 per foot (7.87×10^6 /m). Boundary-layer profiles were measured at four stations which were spaced at distances up to 18 feet (5.5 m) from the plate leading edge. The data obtained for the two protuberance configurations were compared with that obtained over a smooth flat plate. The results of the investigation revealed that both configurations of protuberances were effective in thickening the boundary layer. However, the conical protuberances produced thicker boundary layers with less flow distortion within the boundary layer.

INTRODUCTION

In the design of supersonic-cruise aircraft it can be advantageous to nacelle mount the engines with the inlets located underneath the aircraft's wing. This type of installation may provide favorable interference between the nacelle and wing flow fields, and it offers the inlet important shielding from changes in angle of attack. However, locating an inlet near a wing raises the question of wing-boundary-layer effects on the starting and operating characteristics of the inlet.

Wind tunnel investigations of these boundary-layer effects require the simulation of a realistic wing boundary layer. This simulated boundary layer has two basic requirements. The boundary layer must be fully developed and turbulent with a velocity profile

similar to that expected on an actual aircraft's wing. In addition, the ratio of the boundary-layer thickness to the inlet model size must be the same as that of the full-scale aircraft.

The natural boundary-layer growth on a flat plate may be inadequate for wind tunnel testing of some aircraft configurations because of the excessive plate length required. In many types of tunnel tests the leading-edge surface is roughened to ensure a turbulent boundary layer and to increase the boundary-layer thickness over the plate (refs. 1 and 2). However, roughening techniques are not well defined and may not produce a thick enough boundary layer. By protruding obstacles into the free stream above the plate a localized momentum loss is created which generates much thicker boundary layers downstream of these protuberances (ref. 3). However, sufficient length is required between the protuberances and the station where the inlet is located so that the flow distortion created by the protuberances can be smoothed by mixing effects.

In the present study two protuberance configurations were designed to generate an artificially thickened wing boundary layer on a flat plate for future inlet studies in the Lewis 10- by 10-Foot Supersonic Wind Tunnel. The purpose of this test was to investigate the development of boundary-layer characteristics generated by these designs and to determine whether they are a reasonable simulation of a natural boundary layer.

APPARATUS AND PROCEDURE

Model

The test model was a flat plate 18 feet (5.5 m) in length with a sharp leading edge which was mounted horizontally in the test section and supported by ceiling struts. A sketch of the details of this plate and its installation in the wind tunnel are shown in figure 1. The flat-plate model had removable leading-edge sections 5 inches (12.7 cm) deep, which were used to change the boundary-layer-generating configurations during the investigation. The three model configurations investigated were designated as follows:

- Configuration (1): Smooth flat plate, no protuberances on the plate's leading-edge sections (fig. 2(a))
- Configuration (2): Cylindrical generators, an arrangement of four rows of staggered cylindrical protuberances mounted on the leading-edge sections (fig. 2(b))
- Configuration (3): Conical generators, an arrangement of two rows of staggered biconical protuberances mounted on the leading-edge sections (fig. 2(c))

A leading-edge section of each configuration is shown in figure 3.

The design of these boundary-layer generators was based on equating the drag or

momentum loss of the protuberances with that of the desired wing boundary layer. The two protuberance configurations were designed with the philosophy to distribute the initial momentum loss (a) in the manner of a one-seventh-power-law boundary layer profile and (b) in an equivalent step profile (fig. 4). In order to estimate the distance required behind the generators to achieve a well developed turbulent boundary layer, a Sasman and Cresci turbulent boundary-layer program (ref. 4) was used to investigate the turbulent boundary-layer development on a flat plate. The theoretical growth of the compressible shape parameter is presented in figure 5, for two boundary layers with equal initial momentum losses. Curve A is initially a well-developed turbulent profile (HI = 1.3), whereas curve B is initially at the point of boundary-layer separation (HI = 2.6). As can be seen in the figure, the boundary-layer profile is independent of its initial profile for plate lengths greater than 100 inches (254 cm). Therefore, the initial momentum loss distribution of the generators would not be expected to affect the boundary-layer profile at distances greater than 100 inches (254 cm).

The desired boundary layer that was selected for the design of the boundary-layer generators was a turbulent boundary layer with a thickness of 3.1 inches (7.88 cm) and a one-seventh-power-law velocity profile. Thus,

$$\frac{u}{u_e} = \left(\frac{y}{\delta}\right)^{1/N} \quad (1)$$

where $N = 7$. (Symbols are defined in appendix A.)

The drag (per unit width) of a boundary layer on a flat plate is defined as

$$\text{Drag} = \int_0^{\delta} \rho u (u_e - u) dy \quad (2)$$

Thus, the boundary-layer drag is a function of the free-stream conditions and the momentum thickness of the boundary layer:

$$\text{Drag} = \rho_e u_e^2 \int_0^{\delta} \frac{\rho}{\rho_e} \frac{u}{u_e} \left(1 - \frac{u}{u_e}\right) dy \quad (3)$$

In order to simplify the integration of the momentum thickness integral and, moreover, the design of the protuberances, an assumption of incompressibility was made ($\rho = \rho_e$). With the design of the protuberances based on the incompressible momentum thickness, a thicker compressible boundary layer would be expected. However, with both pro-

tubercle configurations designed with the same incompressible premise, relative comparisons are considered reasonable. Combining equations (1) and (3) and using the incompressible assumption, the following relation was obtained:

$$\text{Drag} = \rho_e u_e^2 \int_0^{\delta} \left(\frac{y}{\delta}\right)^{1/N} \left[1 - \left(\frac{y}{\delta}\right)^{1/N}\right] dy \quad (4)$$

Upon integration,

$$\text{Drag} = (\rho_e u_e^2) \left[\frac{N}{(N+1)(N+2)} \delta \right] \quad (5)$$

The cylindrical protuberance configuration was an arrangement of right-circular cylinders mounted normal to the plate surface. The drag of each cylindrical protuberance can be calculated by

$$\text{Drag} = \frac{1}{2} \rho_e u_e^2 C_D A \quad (6)$$

where C_D was assumed to be 1.25 for a cylindrical protuberance and A is the frontal area of the cylinder. Therefore, the total drag per unit width is

$$\text{Drag} = \frac{n}{2} \rho_e u_e^2 C_D (2Rh) \quad (7)$$

where

R radius of cylindrical protuberances

h height of cylindrical protuberances

n number of cylindrical protuberances per unit width

Equating the boundary-layer drag (eq. (5)) to the cylindrical protuberance drag (eq. (7)) yields

$$C_D nRh = \frac{N}{(N+1)(N+2)} \delta \quad (8)$$

For a given boundary-layer thickness δ and a boundary-layer velocity profile N , a series of cylindrical protuberance configurations could be used to generate the desired boundary layer.

According to reference 5 a supersonic flow separation and a local subsonic reverse-flow zone are formed upstream of cylindrical protuberances. The shape and extent of this separation are a function of the diameter of the cylindrical protuberances. In an attempt to minimize these separation effects, the diameter of the cylinders was chosen to be 0.125 inch (0.317 cm). In order to avoid local overcontraction of passages between cylinders, adjacent cylinders were located on 1.0-inch (2.54-cm) centers with rows 1.0 inch (2.54 cm) apart.

In concept, the conical protuberance configuration was derived from contoured teeth mounted normal to the plate surface. The contoured design was based on the incremental drag (or momentum loss) as a function of distance from the surface y . Hence, at y_i the drag increment in the boundary-layer profile is obtained from equation (3).

$$\Delta\text{Drag} = \rho_e u_e^2 \left(\frac{u_i}{u_e} \right) \left(1 - \frac{u_i}{u_e} \right) \Delta y \quad (9)$$

The drag increment of the protuberance can be obtained from equation (6) by considering a small increment of the contoured protuberance to be approximated by a cylinder with radius R and height of Δy .

$$\Delta\text{Drag} = \frac{1}{2} \rho_e u_e^2 C_D (2R_i \Delta y) \quad (10)$$

The total incremental drag for n protuberances per unit width is

$$\Delta\text{Drag} = \frac{n}{2} \rho_e u_e^2 C_D (2R_i \Delta y) \quad (11)$$

Therefore, by equating the boundary-layer drag increment (eq. (9)) and the contoured protuberance drag increment (eq. (11)), the radius of the contoured protuberance at y_i is

$$R_i = \frac{1}{nC_D} \left(\frac{u_i}{u_e} \right) \left(1 - \frac{u_i}{u_e} \right) \quad (12)$$

Using equation (1), the radius of the contoured protuberance can be defined as a function of y_i :

$$R_i = \frac{1}{nC_D} \left(\frac{y_i}{\delta} \right)^{1/N} \left[1 - \left(\frac{y_i}{\delta} \right)^{1/N} \right] \quad (13)$$

It was again assumed that $C_D = 1.25$. To simplify the fabrication of the contoured protuberance, the desired contour was closely approximated with the biconical shape shown in figure 2(c), which provided the same protuberance drag. The biconical protuberances were located on 2.0-inch (5.08-cm) centers with rows 2.0 inches (5.08 cm) apart.

Instrumentation

The flat-plate model was instrumented with four boundary-layer measuring rakes at the model stations shown in figure 1(a). The details of the rakes are shown in figure 6. Boundary-layer rakes at stations A, B, and C were removed when data were taken with the boundary-layer rake at station D.

Each configuration was tested at three different nominal Mach numbers, $M_w = 2.3$, $M_w = 2.5$ and $M_w = 2.6$. The free-stream Reynolds number was approximately 2.4×10^6 per foot ($7.87 \times 10^6/m$).

Data Reduction

The boundary-layer-rake data were reduced with the assumption that the wall static pressure was constant through the boundary layer. Mach number profiles were computed the usual way: In subsonic flow from the isentropic relation,

$$\frac{P_t}{P} = \left(1 + \frac{\gamma - 1}{2} M^2 \right)^{\gamma/(\gamma-1)} \quad (14)$$

In supersonic flow from the Rayleigh pitot formula,

$$\frac{P_t}{P} = \left(\frac{\gamma + 1}{2} M^2 \right)^{\gamma/(\gamma-1)} \left[\frac{(\gamma + 1)}{2\gamma M^2 - (\gamma - 1)} \right]^{1/(\gamma-1)} \quad (15)$$

Velocity and density profiles were calculated assuming a temperature distribution through the boundary layer. According to reference 6 a temperature distribution in a compressible turbulent boundary layer can be approximated by

$$\frac{T}{T_e} = \frac{T_w}{T_e} + \left(\frac{T_r}{T_e} - \frac{T_w}{T_e} \right) \frac{u}{u_e} - \left(\frac{T_r}{T_e} - 1 \right) \left(\frac{u}{u_e} \right)^2 \quad (16)$$

where

$$\frac{T_r}{T_e} = 1 + r \frac{\gamma - 1}{2} M_e^2 \quad (17)$$

This temperature distribution can be simplified by assuming an adiabatic wall temperature ($T_w = T_r$) and the velocity distribution relation

$$\frac{u}{u_e} = \frac{M}{M_e} \left(\frac{T}{T_e} \right)^{1/2} \quad (18)$$

Therefore,

$$\frac{T}{T_e} = \frac{1 + r \frac{\gamma - 1}{2} M_e^2}{1 + r \frac{\gamma - 1}{2} M^2} \quad (19)$$

The boundary-layer displacement thickness δ^* and the boundary-layer momentum thickness θ were determined by integrating the following expressions:

$$\delta^* = \int_0^{\delta} \left(1 - \frac{\rho u}{\rho_e u_e} \right) dy \quad (20)$$

$$\theta = \int_0^{\delta} \frac{\rho u}{\rho_e u_e} \left(1 - \frac{u}{u_e} \right) dy \quad (21)$$

The subscript e refers to the conditions at which $y = \delta$. The boundary-layer thickness δ was determined by the method developed in the appendix of reference 1, where $[1 - (u/u_e)]^{1/2}$ is a linear function of $y^{3/2}$. According to the reference this method gives a more realistic δ so that the displacement thickness and momentum thickness integrations include almost all the momentum loss in the boundary layer.

A starting point of the effective plate length x_e was determined from the Reynolds

number based on the momentum thickness Re_θ at that station. Reference 7 presents a relation between Re_θ and Reynolds number based on distance from the effective start of the turbulent boundary layer Re_x . This relation is

$$Re_\theta = 0.228 \frac{T_e}{T^*} Re_x \left\{ \log_{10} \left(\frac{T_e \mu_e}{T^* \mu^*} Re_x \right) \right\}^{-2.58} \quad (22)$$

The asterisk indicates an intermediate enthalpy condition where

$$T^* = 0.35 T_e + 0.65 T_r \quad (23)$$

The local skin friction coefficient was calculated by the method also reported in reference 7:

$$C_f = 0.288 \frac{T_e}{T^*} \left\{ \log_{10} \left(\frac{T_e \mu_e}{T^* \mu^*} Re_x \right) \right\}^{-2.45} \quad (24)$$

This method was developed for a compressible turbulent boundary layer, assuming a recovery factor of 0.890.

A summary of the boundary-layer parameters for all the configurations investigated are presented in table I.

RESULTS AND DISCUSSION

Boundary-Layer Profiles

The boundary-layer velocity profiles for the three configurations are presented in figures 7 to 9, respectively. The data are presented such that a comparison of the boundary-layer profiles at the four measuring stations on the plate can be made for each nominal Mach number tested. The boundary-layer profiles generated by the cylinders (fig. 8) were quite irregular at the first rake station but improved at further aft locations. The boundary-layer profiles of the conical generators (fig. 9) also showed a transition to a well-developed turbulent boundary-layer profile; however, their profiles seemed to be better developed at plate station A than those of the cylindrical generators. The profiles at station A of the conical generators were further improved with increases in Mach number.

For a comparison of the velocity profiles of the three configurations investigated, the data were nondimensionalized to their own boundary-layer thickness δ . Figures 10 to 12 present these data for the three nominal Mach numbers investigated - 2.3, 2.5, and 2.6, respectively. Each figure shows the comparison of the three configurations and the theoretical one-seventh power-law profile at each boundary-layer measuring station.

At the four plate stations, characteristic boundary-layer profile trends were observed for each of the three configurations investigated. At station A, the generated boundary-layer profiles differed significantly from the theoretical one-seventh power profile, with the boundary layer generated by the cylinders having an excess of momentum loss and the boundary layer generated by the cones having a deficit of momentum loss in the boundary layer. The natural boundary layer was almost coincident with the theoretical profile. At station B, better development had occurred in both generated boundary-layer profiles. The profiles generated by the cylinders had completed a transition to a fully developed turbulent boundary layer; however, the profile still had an excess of momentum loss in comparison to the theoretical profile. The profiles generated by the cones had become almost coincident with the theoretical profile.

At station C and station D, the profiles generated by the cylinders continued to approach the theoretical one-seventh power profile; however, they never actually attained it because of a characteristic "flatness" to the profile. The profiles generated by the cones became essentially coincident with the theoretical profile at station C. No data were recorded at station D for the conical generators.

Boundary-Layer Thickness Parameters

The growth of the boundary layers along the plate is presented in terms of three boundary-layer thickness parameters:

- (1) Boundary-layer thickness, δ
- (2) Displacement thickness, δ^*
- (3) Momentum thickness, θ

The comparison of the three boundary-layer configurations for each of these parameters is presented in figures 13 to 15. The three figures present results obtained at the three nominal Mach numbers investigated - 2.3, 2.5, and 2.6, respectively.

The growth of the boundary-layer thickness parameters along the plate for the smooth flat plate configuration was consistent with normal boundary-layer growth predictions. Also the growth trends of the thickness parameters were constant within the Mach number range.

The boundary-layer thickness δ along the plate for the cylindrical generators assumed a growth trend parallel to the natural boundary layer and was approximately 1.5 inches (3.8 cm) thicker. The displacement and momentum thicknesses of the generated boundary layer indicated an unusual growth trend at $M_w = 2.3$ but developed a more consistent trend at the higher Mach numbers.

The boundary-layer thickness δ along the plate for the conical generators assumed a growth trend which was 4.1 inches (10.4 cm) thicker than the natural boundary layer at station A, 3.6 inches (9.1 cm) thicker at station B, and 3.0 inches (7.6 cm) thicker at station C. The displacement and momentum thicknesses of the same boundary layer had growth trends which were parallel to those of the natural boundary layer and were constant within the Mach number range investigated.

Boundary-Layer Shape Parameters

A comparison of the growth of the boundary-layer shape parameter H along the plate for the three configurations is shown in figure 16. The figure is divided into three parts, one for each of the three nominal Mach numbers investigated. The boundary-layer shape parameter indicated characteristic growth trends for each of the three configurations. By comparing the two artificially generated boundary layers with the natural boundary layer it is apparent that the boundary layer generated by the cylinders provided a closer approximation to the natural boundary layer. However, results from all three configurations converged near the end of the plate.

The effect of Mach number on the boundary-layer shape parameter H for a one-seventh power-law velocity profile is given in figure 17. Because of the large variation of H with Mach number, the absolute numerical value of H in compressible flow loses the significance it has in incompressible flow. Therefore, a normalized boundary-layer shape parameter K_H was adopted, where

$$K_H = \frac{H}{H_{N=7}} \quad (25)$$

And $H_{N=7}$ in the preceding equation was obtained from figure 17. This normalized parameter is independent of Mach number and also defines the shape relative to the design one-seventh power-law velocity profile.

The normalized boundary-layer shape parameters for all configurations investigated are shown in figure 18. As stated before, the boundary layer generated by the cylinders was a closer approximation to the natural boundary layer than that of the conical generators in this type of comparison.

Boundary-Layer Power Profile Parameter

A comparison of the growth of the boundary-layer power profile parameter N along the plate for the three boundary-layer configurations is shown in figure 19. The figure is divided into three parts for the three Mach numbers tested. The power profile parameter of the natural boundary layer varied between a seventh- and eighth-power profile along this plate and showed little effect of Mach number. The power profile parameter of the boundary layer generated by the cylinders was significantly less, but tended to converge at further-aft stations toward the natural boundary-layer results. The power profile parameter of the boundary layer generated by the cones indicated a better correlation with the natural boundary layer, particularly at the higher Mach numbers.

Similar to the normalized boundary-layer shape parameter K_H , a normalized boundary-layer power profile parameter was defined as

$$K_N = \frac{N}{7} \quad (26)$$

The normalized boundary-layer power profile parameter for all configurations investigated is shown in figure 20. The boundary layer generated by the cones shows a better correlation to the natural boundary layer at all locations downstream of station A.

The separation characteristics of the boundary layer generated by the cylinders were evaluated by means of a forward-facing step. The details and results of this investigation are presented in appendix B.

Effective Flat-Plate Length

Determination of an effective increase in flat-plate length produced by the artificially thickened boundary layers is important for scaling aspects. Since a portion of the momentum deficit of the generated boundary layers was artificially induced at the leading edge of the plate, an increase in flat-plate length would be required to produce a natural boundary layer with the same characteristic growth over the plate.

A correlation of the effective increase in flat-plate length for the three configurations and the three nominal Mach numbers is shown in figure 21. The calculations for the flat-plate configuration, which generated a natural boundary layer, indicated an average effective plate length slightly shorter than the actual plate length. However, this calculation neglected the natural transition from laminar to turbulent boundary layer which was expected at approximately 20 inches (50.8 cm) from the leading edge. The effective plate length for the natural boundary layer was completely independent of the

Mach number. However, the effective plate length using the cylindrical generators was not independent of Mach number. At Mach 2.3, the effective increase in plate length was 165 inches (419 cm); and at Mach 2.5, the effective increase was 207 inches (525.8 cm). Data were insufficient for a correlation at Mach 2.6. The conical generators produced an effective increase in plate length of approximately 312 inches (792.5 cm), which tended to be constant with Mach number.

SUMMARY OF RESULTS

Measurements were made of the turbulent-boundary-layer profiles which were artificially thickened by protuberances on the leading edge of a flat plate. Two configurations of protuberances were investigated: a configuration of cylindrical protuberances and a configuration of biconical protuberances. The Mach number range investigated was $M_w = 2.3$ to $M_w = 2.6$ and the free-stream Reynolds number was 2.4×10^6 per foot ($7.87 \times 10^6/m$). Results were compared to a natural boundary layer on the flat plate.

A comparison of the boundary-layer velocity profiles was made at four stations which were spaced at distances up to 18 feet (5.5 m) from the plate's leading edge. The following results were obtained:

1. Both protuberance configurations were effective in generating an artificially thickened boundary layer. However, the conical protuberances produced thicker boundary layers with less flow distortion in the boundary layer than the cylindrical protuberances.
2. The boundary layer generated by the cylinders had an excess of momentum loss in proportion to its height at stations upstream on the plate but approached a seventh-power-law velocity profile with increased plate length. However, a characteristic "flatness" in the boundary-layer profile was apparent at all stations. In contrast, the boundary layer generated by the cones had a deficit of momentum loss in proportion to its height at the upstream station and became essentially coincident with the seventh-power profile at half the plate's length.
3. The cylindrical protuberances generated a boundary layer which was approximately 1.5 inches (3.8 cm) thicker than the natural boundary layer. The conical protuberances generated a boundary layer which was 3.0 inches (7.6 cm) thicker than the natural boundary layer at the aft measuring station.
4. The boundary-layer shape parameter H exhibited individual growth trends along the plate for the three configurations. However, a convergence of the individual trends was apparent with sufficient length. In reference to the shape parameter development, the boundary layer generated by the cylinders revealed a better approximation to the natural boundary-layer development.

5. The boundary-layer velocity power profile parameter N also exhibited individual growth trends along the plate for the three configurations. However, the results obtained with the conical generators generally provided a better approximation to the natural boundary-layer development.

Lewis Research Center,
National Aeronautics and Space Administration,
Cleveland, Ohio, November 25, 1970,
720-03.

APPENDIX A

SYMBOLS

A	frontal area, in. ² (cm ²)	u	velocity, in./sec (cm/sec)
C _D	coefficient of drag	x	distance from leading edge of plate, in. (cm)
C _f	local skin friction coefficient	x _e	effective distance from leading edge of plate, in. (cm)
H	boundary-layer shape parameter, δ^*/θ	x'	distance forward of forward-facing step, in. (cm)
HI	incompressible shape parameter	y	distance normal to plate surface, in. (cm)
h	height of protuberance, in. (cm)	γ	specific-heat ratio
h _s	forward-facing step height, in. (cm)	δ	boundary-layer thickness, in. (cm)
K _H	normalized boundary-layer shape parameter	δ^*	boundary-layer displacement thickness, in. (cm)
K _N	normalized boundary-layer power profile parameter	θ	boundary-layer momentum thickness, in. (cm)
M	Mach number	μ	viscosity, lbm/ft-sec (N-sec/m ²)
M _w	nominal Mach number	ρ	density, lbm/ft ³ (kg/m ³)
N	boundary-layer power profile parameter	Subscripts:	
n	number of protuberances per unit width	e	conditions at the edge of boundary layer (y = δ)
P	pressure, lb/ft ² (N/m ²)	i	conditions at arbitrary distance normal to plate surface
R	radius of protuberance, in. (cm)	p	start of plateau or plateau value
Re _x	Reynolds number based on x _e , $\rho u x_e / \mu$	s	separation point
Re _{θ}	Reynolds number based on θ , $\rho u \theta / \mu$	t	stagnation condition
r	recovery factor 0.890	0	conditions in free stream
T	temperature, K (°R)		
T _r	adiabatic wall temperature, K (°R)		
T _w	wall temperature, K (°R)		

APPENDIX B

FORWARD-FACING-STEP INVESTIGATION

The separation of a turbulent boundary layer ahead of an obstacle such as a forward-facing step is a phenomenon of technical importance in evaluating an artificially thickened boundary layer. Because the boundary layer generated by the cylinders was later used in a wing-boundary-layer and inlet-shock interaction test, it was necessary to establish the validity of the separation characteristics of this type of boundary-layer generation.

The installation of a forward-facing step and associated static-pressure instrumentation on the flat-plate model is shown in figure 22. The forward-facing step was located 159 inches (403 cm) from the plate's leading edge. The boundary layer generated by the cylinders had a thickness of approximately 3.5 inches (8.88 cm) at this location.

A correlation of experiments describing the steady pressure field produced by the separation of the turbulent boundary layer ahead of a forward-facing step is presented by Zukoski (ref. 8). The general features of a typical separated flow are shown in figure 23, where a sketch of the principal flow regions is shown with a wall pressure profile.

Plate static-pressure distributions ahead of the forward-facing step were measured at the three nominal Mach numbers tested. The distributions are compared in figure 24 with correlations of the data on natural boundary-layer separation characteristics of reference 8. At Mach number 2.3, the measured pressure distribution was almost identical with predictions for a natural boundary layer. However, there was greater deviation at the higher Mach numbers. The plateau pressure ratio P_p/P_0 of the artificial boundary layer was independent of Mach number; whereas, the prediction is

$$\frac{\Delta P_p}{P_0} \approx \frac{M_0}{2}$$

In addition, the separation point x'_s increased slightly with a corresponding increase in Mach number, which is contrary to the prediction that it would be independent of the Mach number and only a function of the step height.

REFERENCES

1. Peterson, John B., Jr.: Boundary-Layer Velocity Profiles Downstream of Three-Dimensional Transition Trips on a Flat Plate at Mach 3 and 4. NASA TN D-5523, 1969.
2. Samanich, N. E.; Barnett, D. O.; and Salmi, R. J.: Effect of External Boundary Layer on Performance of Axisymmetric Inlet at Mach Numbers of 3.0 and 2.5. NACA TM X-49, 1959.
3. Clever, William W.: Results of an Experimental Turbulent Boundary Layer Control Investigation. NASA TM X-53899, 1969.
4. Sasman, Philip K.; and Cresci, Robert J.: Compressible Turbulent Boundary Layer with Arbitrary Pressure Gradient and Heat Transfer. Polytechnic Inst. Brooklyn (ARL-65-65, AD-615608), Apr. 1965.
5. Voitenko, D. M.; Zubkov, A. I.; and Panov, Iu. A.: Supersonic Gas Flow Past a Cylindrical Obstacle on a Plate. Akad. Nauk SSSR, Izv., Mekh. Zhid. i Gaza, no. 1, Jan.-Feb. 1966, pp. 121-125.
6. Schlichting, Hermann (J. Kestin, trans.): Boundary-Layer Theory. Sixth ed., McGraw-Hill Book Co., Inc., 1968.
7. Smith, K. G.: Methods and Charts for Estimating Skin Friction Drag in Wind Tunnel Tests with Zero Heat Transfer. Rep. CP-824, Aeronautical Research Council, Great Britain, 1965.
8. Zukoski, Edward E.: Turbulent Boundary-Layer Separation in Front of a Forward-Facing Step. AIAA J., vol. 5, no. 10, Oct. 1967, pp. 1746-1753.

TABLE I. - SUMMARY OF PARAMETERS FROM PROFILE MEASUREMENTS

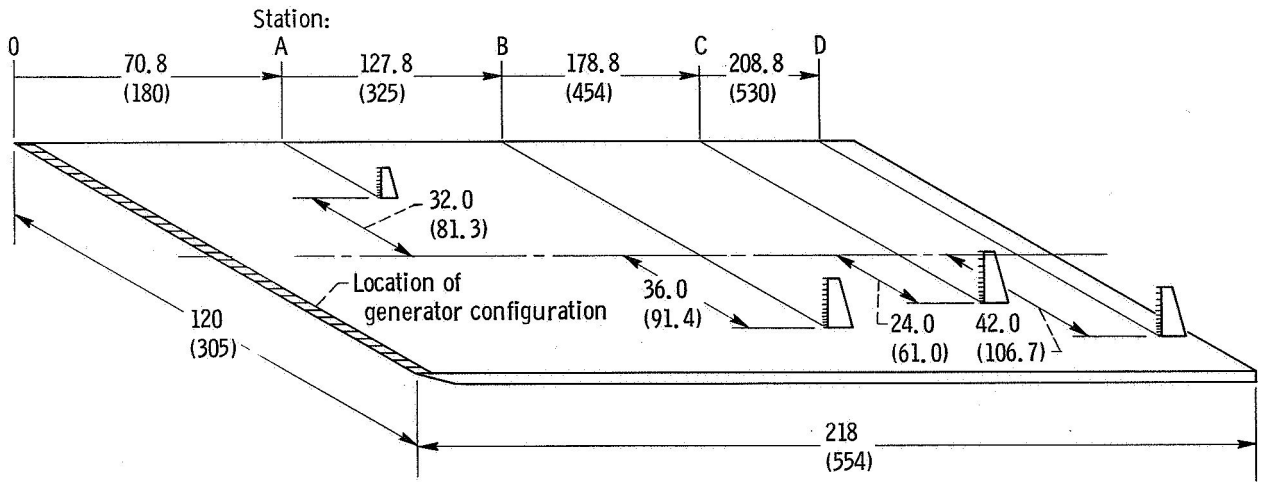
(a) U.S. customary units

Config-uration	x, in.	M ₀	M _e	δ, in.	δ*, in.	θ, in.	H	K _H	N	Re _θ ×10 ⁻⁴	C _f ×10 ³	x _{e'} in.
NAT GEN	70.8	2.346	2.273	0.908	0.213	0.056	3.811	1.142	7.067	1.080	1.758	61.4
NAT GEN	127.8	2.346	2.304	1.719	0.391	0.109	3.575	1.054	7.770	2.107	1.538	115.4
NAT GEN	178.8	2.346	2.229	2.375	0.539	0.159	3.385	1.029	7.258	3.172	1.459	178.3
NAT GEN	203.8	2.346	2.289	2.512	0.546	0.158	3.444	1.024	6.324	3.152	1.437	179.9
NAT GEN	70.8	2.549	2.503	0.885	0.215	0.050	4.295	1.139	7.226	0.958	1.491	47.7
NAT GEN	127.8	2.549	2.515	1.703	0.415	0.104	3.983	1.050	7.806	1.997	1.466	115.3
NAT GEN	178.8	2.549	2.475	2.384	0.586	0.152	3.852	1.027	7.092	2.988	1.378	180.1
NAT GEN	203.8	2.549	2.472	2.480	0.564	0.149	3.781	1.019	6.682	2.920	1.394	174.3
NAT GEN	70.8	2.634	2.594	0.892	0.223	0.050	4.476	1.132	7.241	0.966	1.648	49.8
NAT GEN	127.8	2.634	2.598	1.721	0.431	0.104	4.149	1.047	7.798	2.016	1.431	117.9
NAT GEN	178.8	2.634	2.586	2.381	0.596	0.147	4.066	1.033	7.295	2.981	1.345	177.6
NAT GEN	203.8	2.634	2.559	2.528	0.604	0.153	3.954	1.019	8.560	2.723	1.365	182.5
CYL GEN	70.8	2.299	2.260	2.573	0.834	0.227	3.680	1.111	4.294	4.547	1.359	273.0
CYL GEN	127.8	2.299	2.242	3.080	0.827	0.239	3.464	1.056	5.924	4.701	1.359	287.8
CYL GEN	178.8	2.299	2.197	3.636	0.933	0.280	3.332	1.041	6.441	5.675	1.332	345.0
CYL GEN	203.8	2.309	2.263	3.947	1.026	0.299	3.436	1.025	6.474	5.954	1.298	377.6
CYL GEN	70.8	2.514	2.477	2.528	0.872	0.215	4.057	1.091	4.768	4.200	1.298	271.0
CYL GEN	127.8	2.514	2.469	3.232	1.047	0.261	4.010	1.083	5.146	5.077	1.259	339.8
CYL GEN	178.8	2.514	2.456	3.806	1.118	0.289	3.863	1.051	5.928	5.812	1.235	384.2
CYL GEN	203.8	2.509	2.467	4.165	1.192	0.312	3.824	1.034	6.833	6.178	1.219	419.5
CYL GEN	203.8	2.632	2.559	3.972	1.160	0.290	4.004	1.031	6.965	5.045	1.225	387.2
CUN GEN	70.8	2.346	2.292	5.220	0.942	0.288	3.267	0.965	11.320	5.699	1.297	364.9
CUN GEN	127.8	2.346	2.306	5.558	1.159	0.337	3.435	1.013	7.137	6.639	1.260	439.6
CUN GEN	178.8	2.346	2.244	5.380	1.350	0.393	3.433	1.045	5.806	7.961	1.244	520.5
CUN GEN	70.8	2.549	2.543	4.965	1.058	0.278	2.802	0.988	9.272	5.493	1.217	375.0
CUN GEN	127.8	2.549	2.526	5.382	1.226	0.320	3.830	1.003	7.872	6.242	1.196	439.1
CUN GEN	178.8	2.549	2.499	5.394	1.406	0.366	3.844	1.022	6.702	7.219	1.177	510.8
CUN GEN	70.8	2.635	2.629	5.001	1.106	0.278	3.981	0.989	9.038	5.555	1.185	384.1
CUN GEN	127.8	2.635	2.611	5.346	1.247	0.314	3.973	0.996	8.498	6.172	1.171	439.7
CUN GEN	178.8	2.635	2.542	5.074	1.289	0.330	3.907	1.016	7.064	6.129	1.195	453.0

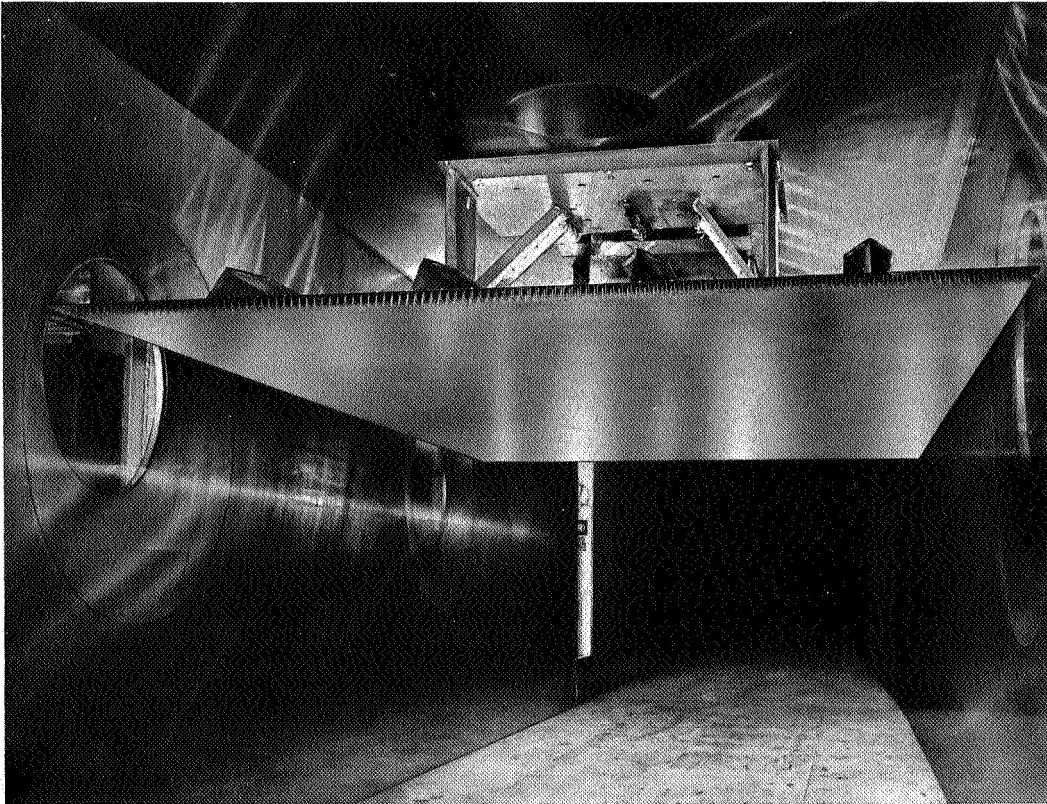
TABLE I. - Concluded. SUMMARY OF PARAMETERS FROM PROFILE MEASUREMENTS

(b) SI units

Config- uration	x_p cm	M_0	M_e	δ , cm	δ^* , cm	θ , cm	H	K_H	N	Re_θ $\times 10^{-4}$	C_f $\times 10^3$	x_e' cm
NAT GEN	179.9	2.346	2.273	2.307	0.542	0.142	3.811	1.142	7.067	1.080	1.758	130.5
NAT GEN	224.7	2.346	2.304	4.366	0.992	0.277	3.575	1.054	7.770	2.107	1.538	293.2
NAT GEN	454.2	2.346	2.229	6.032	1.370	0.405	3.385	1.039	7.258	3.172	1.459	452.8
NAT GEN	530.4	2.346	2.289	6.379	1.386	0.402	3.444	1.024	8.324	3.152	1.437	456.9
NAT GEN	179.9	2.549	2.503	2.248	0.546	0.127	4.295	1.139	7.226	0.958	1.691	121.2
NAT GEN	224.7	2.549	2.515	4.327	1.053	0.264	3.983	1.050	7.806	1.997	1.466	292.8
NAT GEN	454.2	2.549	2.475	6.055	1.489	0.387	3.852	1.037	7.092	2.988	1.378	457.4
NAT GEN	530.4	2.549	2.472	6.298	1.432	0.379	3.781	1.019	8.688	2.820	1.394	442.8
NAT GEN	179.9	2.634	2.594	2.265	0.567	0.127	4.476	1.132	7.241	0.966	1.648	123.8
NAT GEN	224.7	2.634	2.598	4.372	1.095	0.264	4.145	1.047	7.798	2.016	1.430	299.5
NAT GEN	454.2	2.634	2.586	6.047	1.514	0.372	4.066	1.033	7.295	2.881	1.345	451.1
NAT GEN	530.4	2.632	2.559	6.422	1.535	0.388	3.954	1.019	8.560	2.723	1.365	463.4
CYL GEN	179.9	2.299	2.260	6.536	2.119	0.576	3.680	1.111	4.294	4.547	1.359	693.5
CYL GEN	224.7	2.299	2.242	7.824	2.100	0.606	3.464	1.056	5.924	4.701	1.359	731.0
CYL GEN	454.2	2.299	2.197	9.234	2.371	0.712	3.332	1.041	6.441	5.675	1.332	876.3
CYL GEN	530.4	2.309	2.263	10.024	2.606	0.758	3.436	1.035	6.474	5.954	1.298	959.1
CYL GEN	179.9	2.514	2.477	6.422	2.216	0.546	4.057	1.091	4.768	4.200	1.298	688.2
CYL GEN	224.7	2.514	2.469	8.209	2.661	0.663	4.010	1.083	5.146	5.077	1.259	863.2
CYL GEN	454.2	2.514	2.456	9.667	2.839	0.735	3.863	1.051	5.928	5.812	1.235	975.9
CYL GEN	530.4	2.509	2.467	10.580	3.026	0.791	3.824	1.034	6.833	6.178	1.219	1065.4
CYL GEN	530.4	2.632	2.559	10.088	2.946	0.736	4.004	1.031	6.965	5.045	1.225	983.4
CON GEN	179.9	2.346	2.292	13.259	2.394	0.733	3.267	0.969	11.320	5.699	1.297	926.7
CON GEN	224.7	2.346	2.306	13.609	2.944	0.856	3.439	1.013	7.137	6.639	1.260	1116.5
CON GEN	454.2	2.346	2.244	13.665	3.430	0.999	3.433	1.045	5.806	7.961	1.244	1322.0
CON GEN	179.9	2.549	2.543	12.612	2.688	0.707	3.802	0.988	9.272	5.493	1.217	952.4
CON GEN	224.7	2.549	2.526	13.670	3.114	0.813	3.830	1.003	7.872	6.242	1.196	1115.2
CON GEN	454.2	2.549	2.499	13.700	3.572	0.929	3.844	1.022	6.702	7.219	1.177	1297.4
CON GEN	179.9	2.635	2.629	12.702	2.810	0.706	3.981	0.989	9.038	5.555	1.185	975.7
CON GEN	224.7	2.635	2.611	13.580	3.167	0.797	3.973	0.956	8.498	6.172	1.171	1116.9
CON GEN	454.2	2.635	2.542	12.887	3.275	0.838	3.907	1.016	7.064	6.129	1.195	1150.7



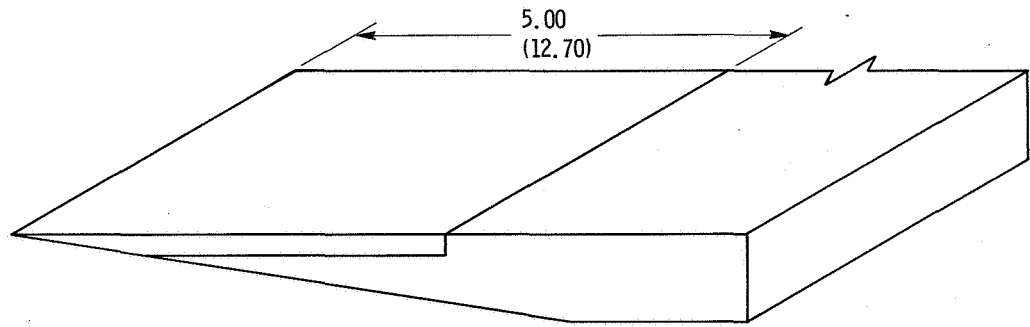
(a) Details and instrumentation of model. (Dimensions in inches (cm).)



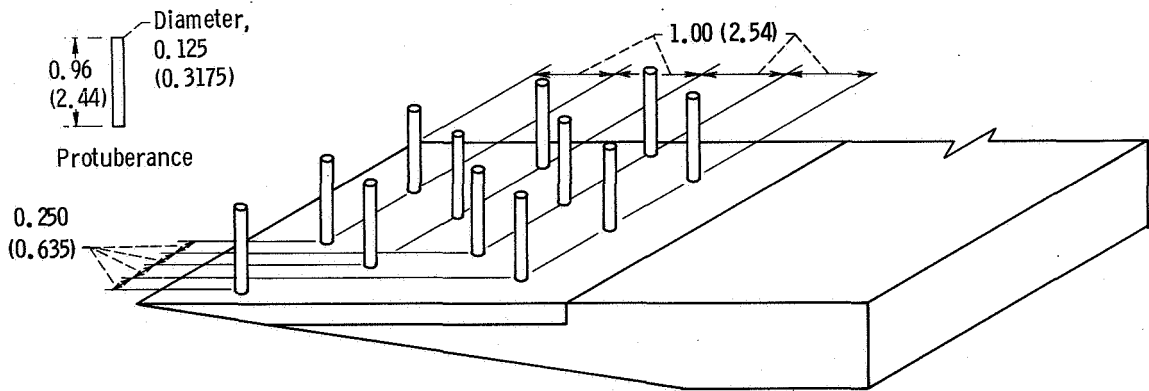
(b) Model installed in wind tunnel.

CD-10816-11

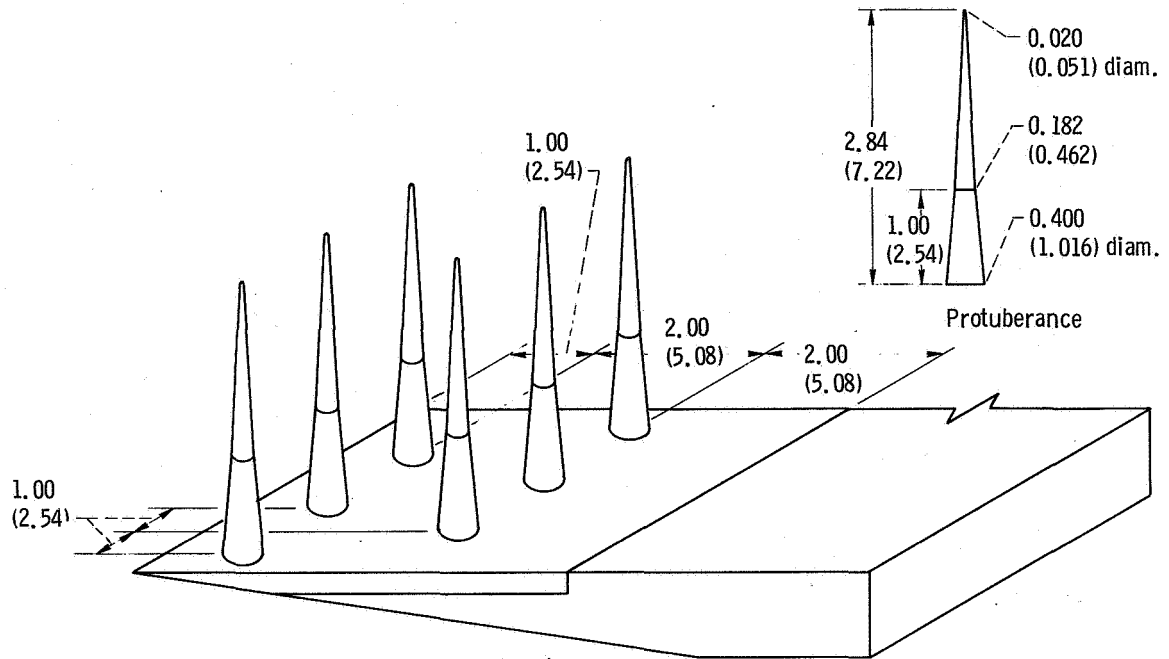
Figure 1. - Flat-plate model.



(a) Leading edge of smooth flat-plate configuration.

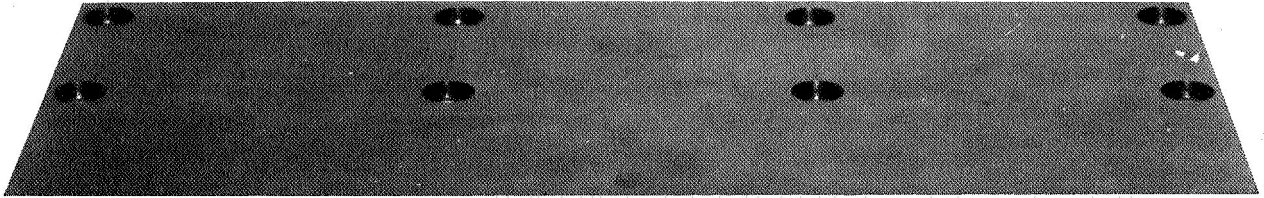


(b) Leading edge of cylindrical generator configuration.



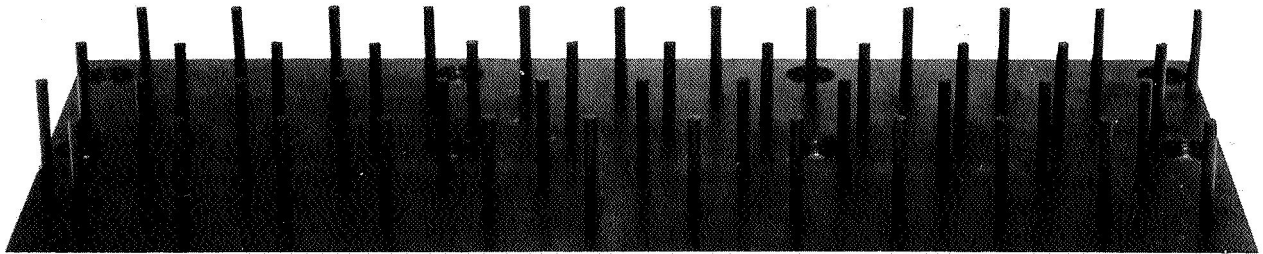
(c) Leading edge of conical generator configuration.

Figure 2. - Details of boundary-layer-generating configurations. (Dimensions are in inches (cm).)



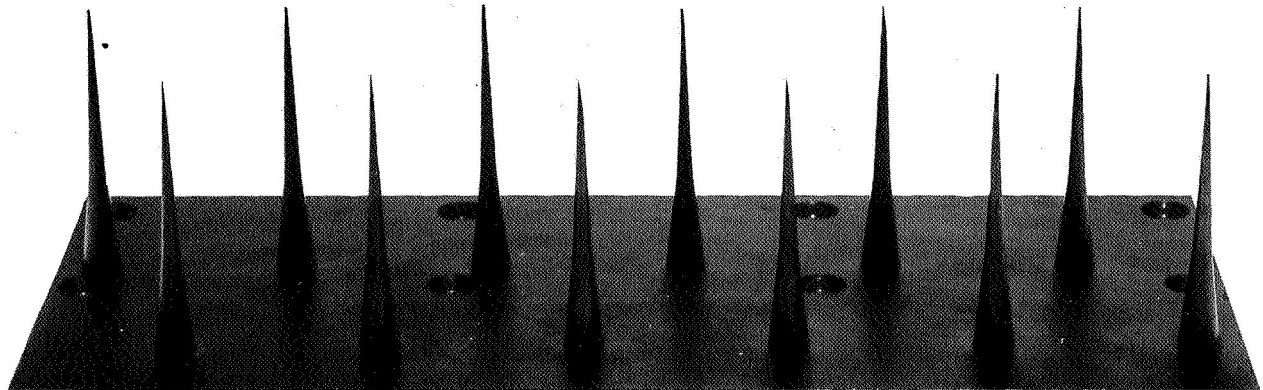
C-70-2186

(a) Smooth flat-plate configuration.



C-70-2187

(b) Cylindrical generator configuration.



C-70-2188

(c) Conical generator configuration.

Figure 3. - Boundary-layer-generating configurations.

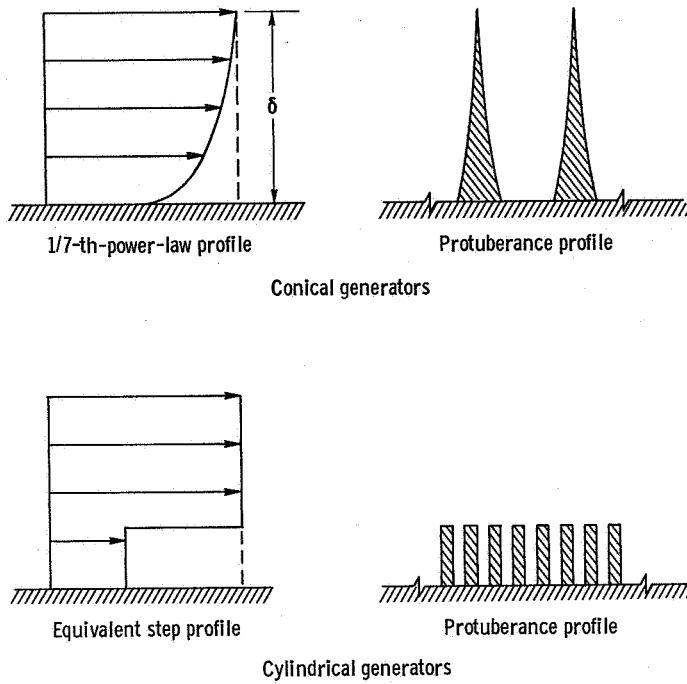


Figure 4. - Design aspects of the boundary-layer generators.

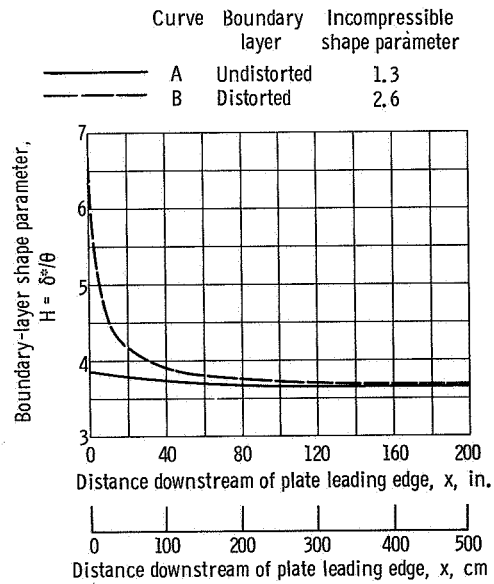


Figure 5. - Theoretical growth of boundary-layer shape parameter on a flat plate. Free-stream Mach number, 2.5; Reynolds number, 2.4×10^6 per foot ($7.87 \times 10^6/m$).

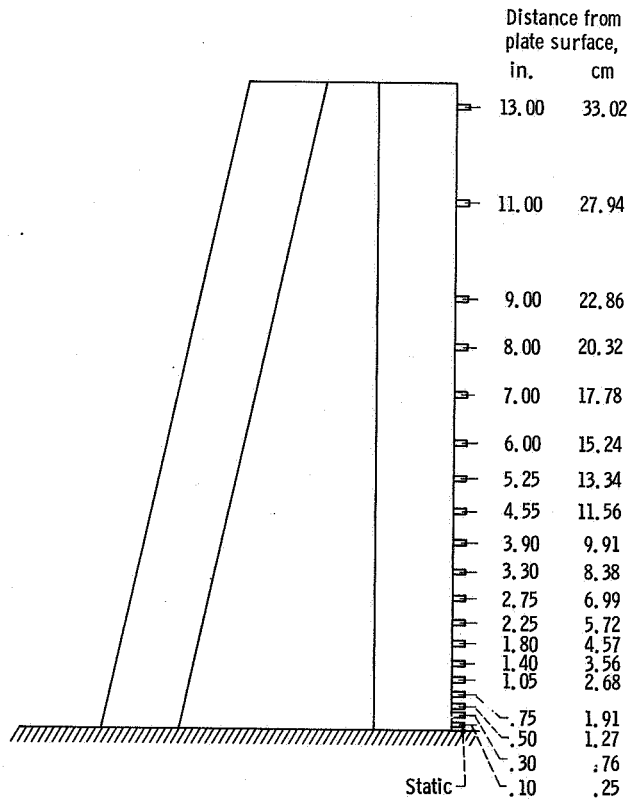


Figure 6. - Boundary-layer-rake instrumentation.

Station	Distance from leading edge of plate, x
	in. cm
○ A	70.8 180
□ B	127.3 325
◇ C	173.8 454
△ D	203.8 530

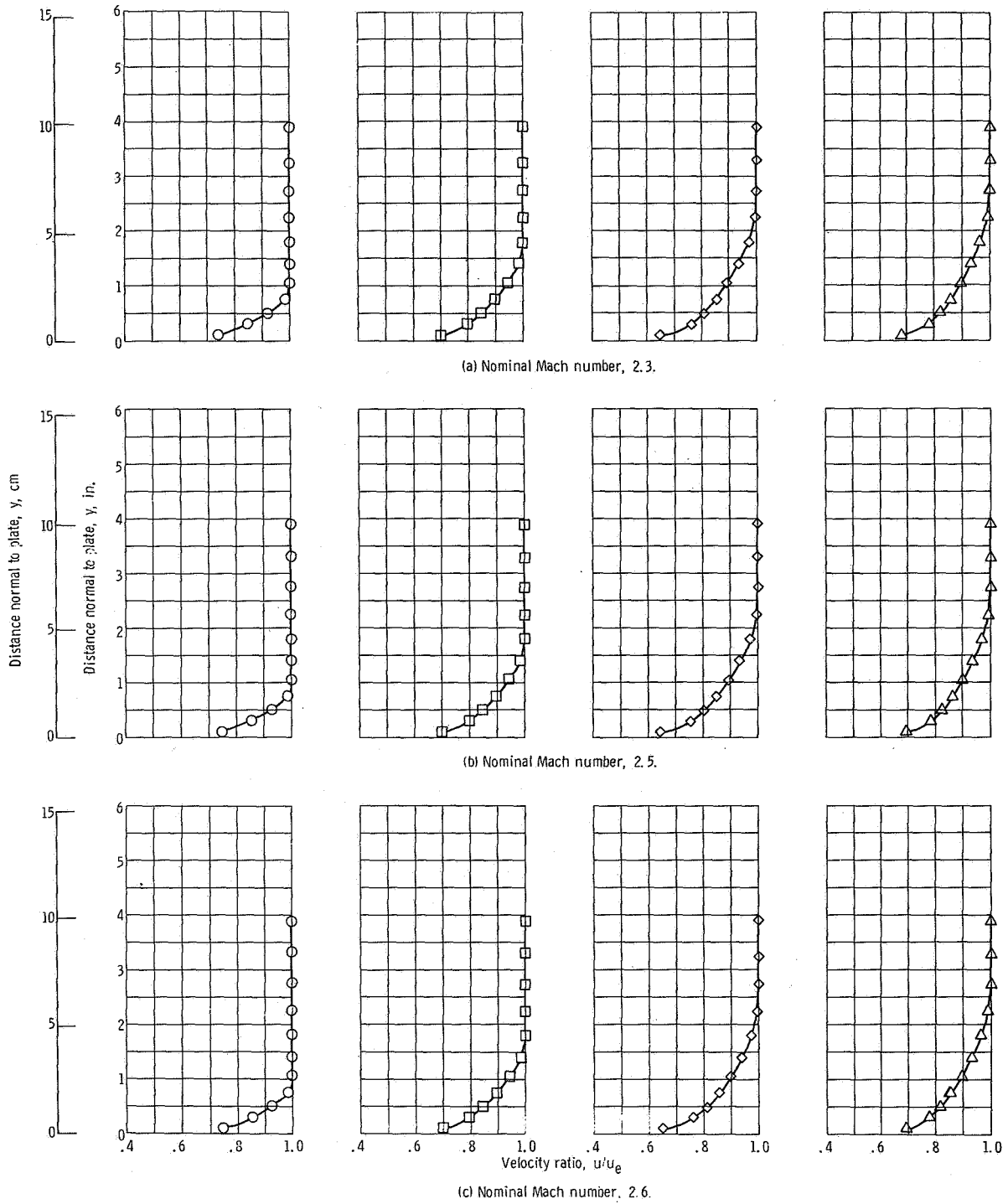


Figure 7. - Boundary-layer velocity profiles with smooth flat plate.

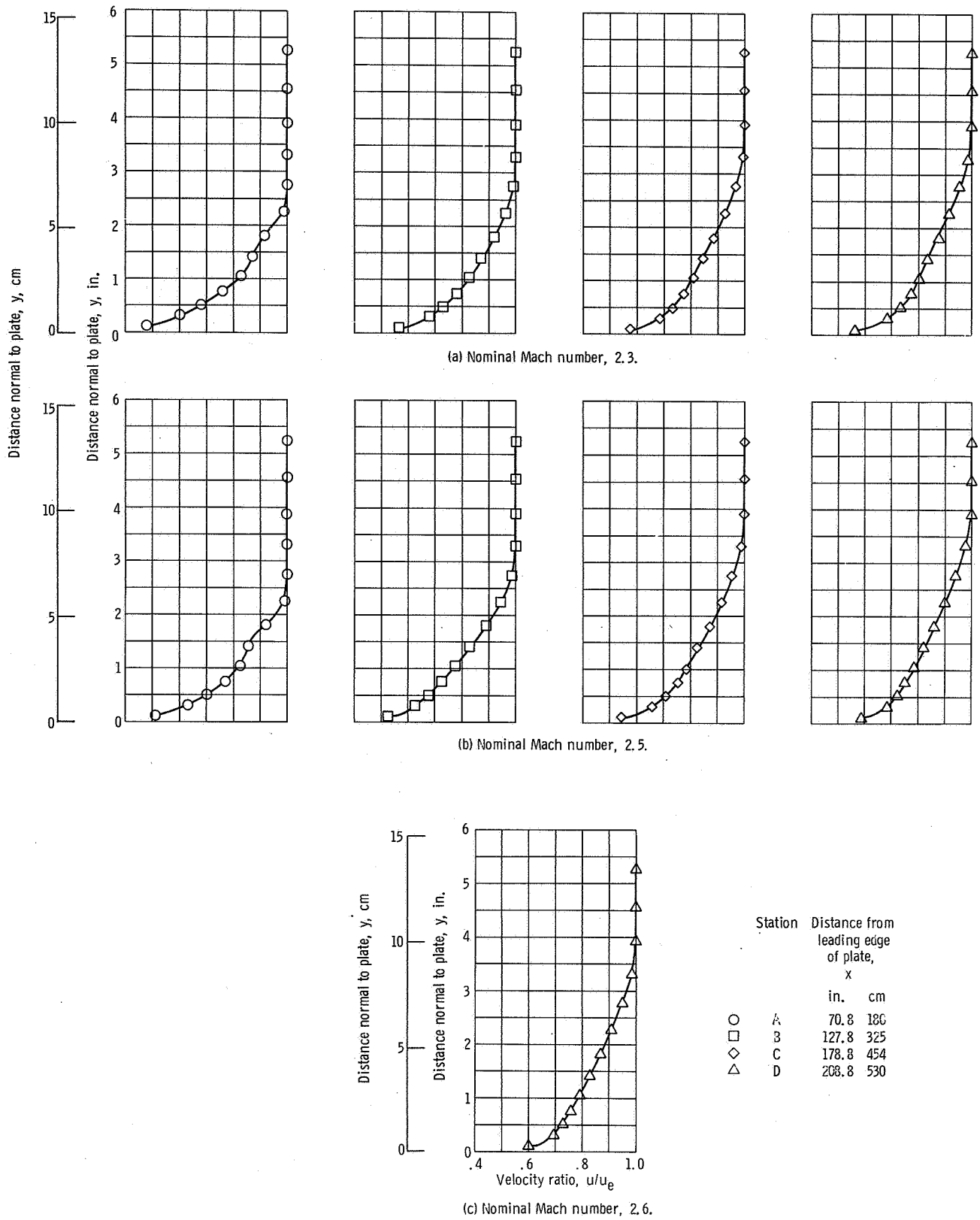


Figure 8. - Boundary-layer velocity profiles with cylindrical generators.

Station	Distance from leading edge of plate, x	
	in.	cm
○ A	70.8	180
□ B	127.8	325
◇ C	178.8	454

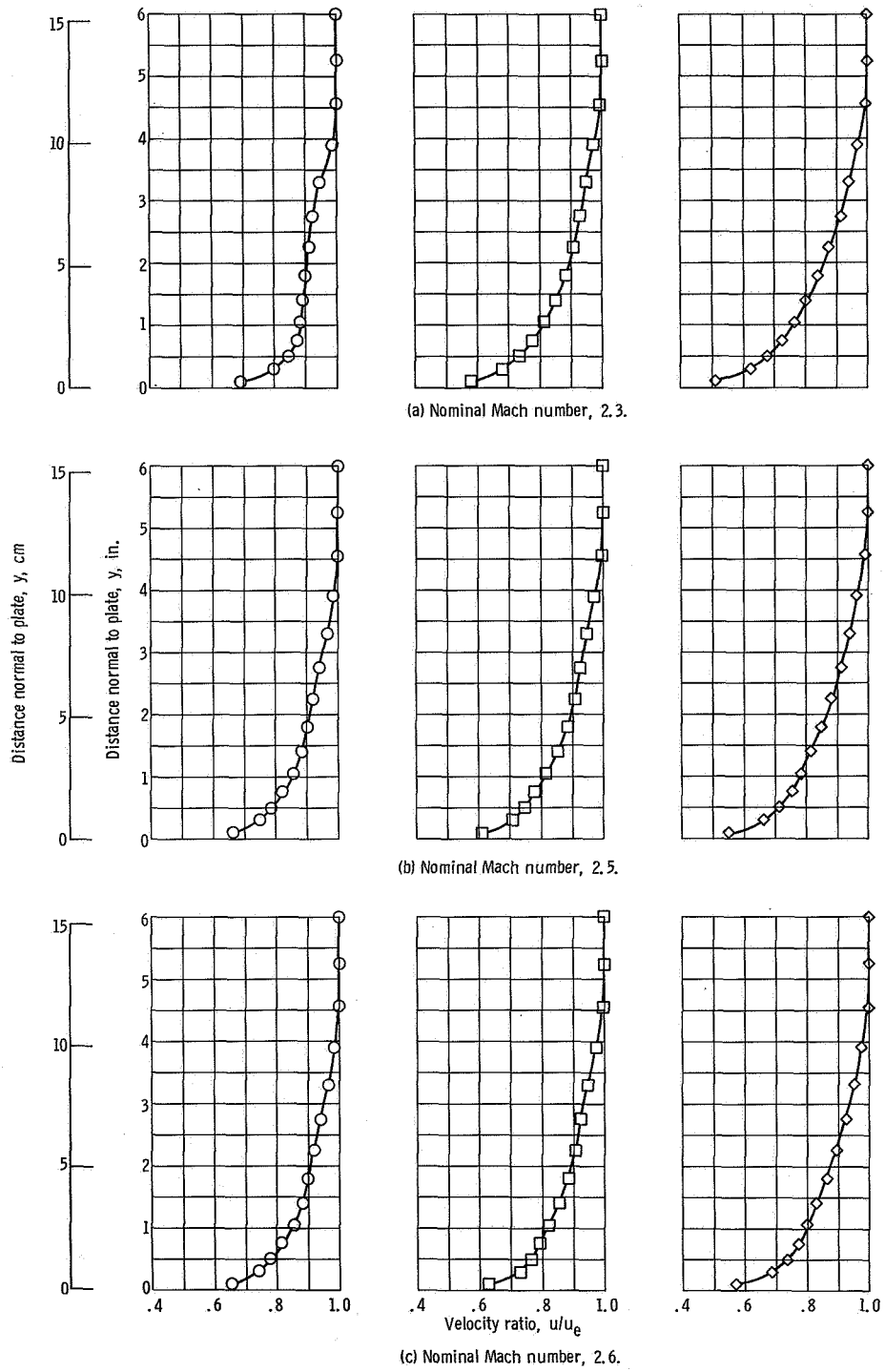


Figure 9. - Boundary-layer velocity profiles with conical generators.

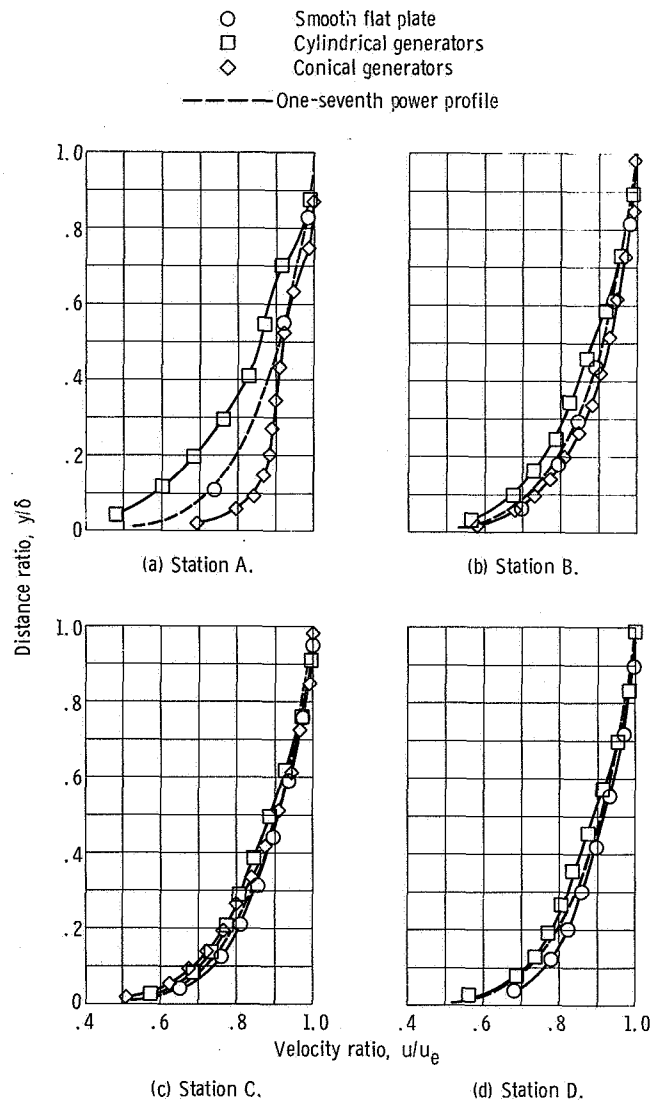


Figure 10. - Comparison of nondimensionalized boundary-layer profiles for nominal Mach number of 2.3.

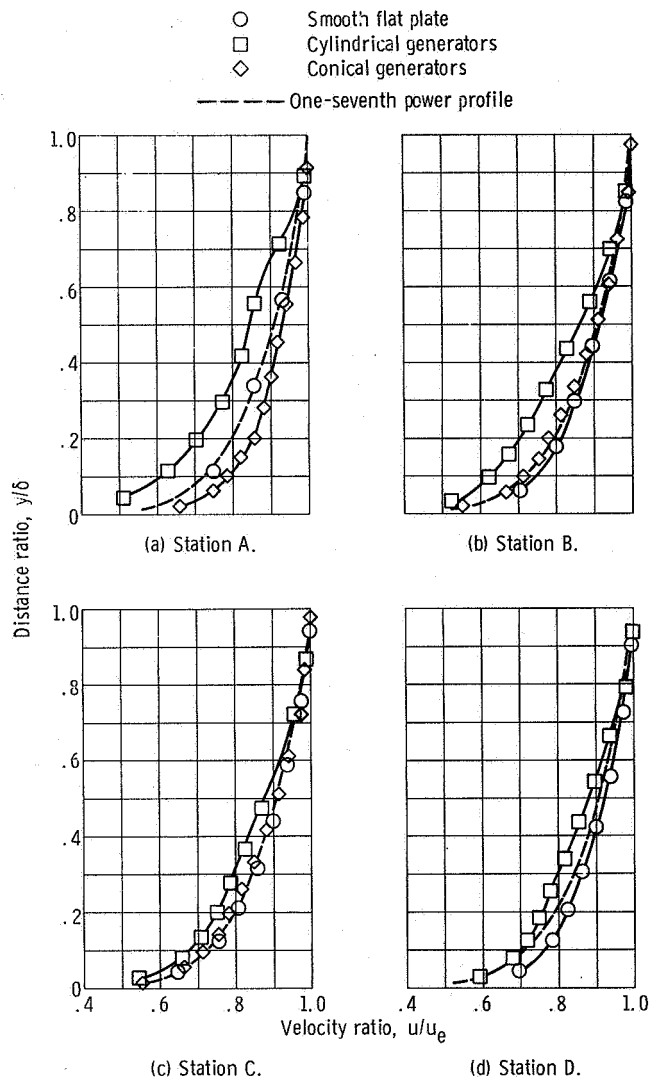


Figure 11. - Comparison of nondimensionalized boundary-layer profiles for nominal Mach number of 2.5.

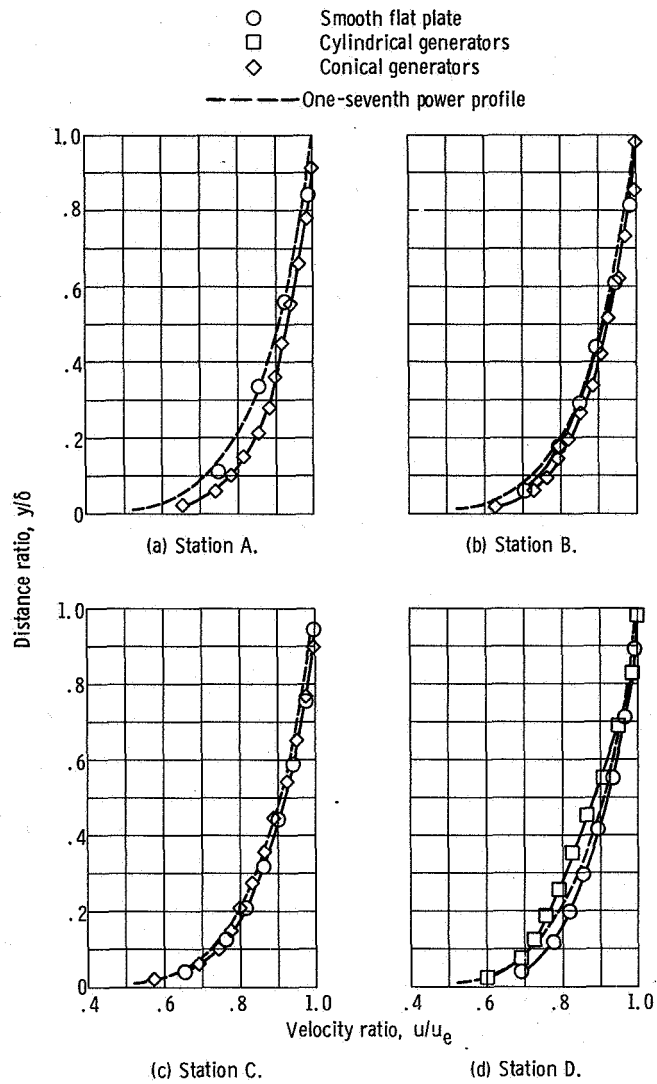


Figure 12. - Comparison of nondimensionalized boundary-layer profiles for nominal Mach number of 2.6.

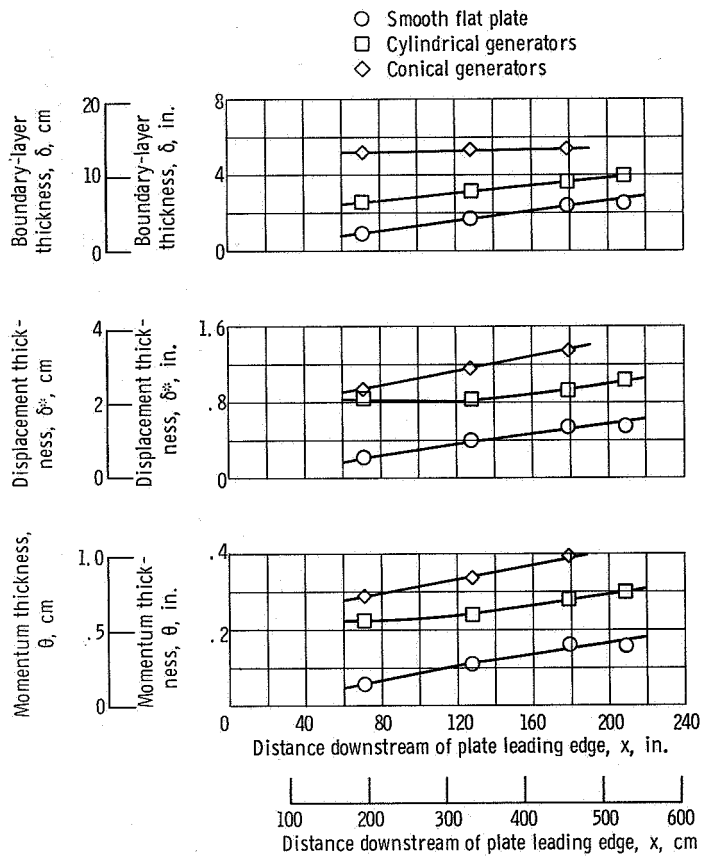


Figure 13. - Comparison of thickness parameters for the three configurations at nominal Mach number of 2.3.

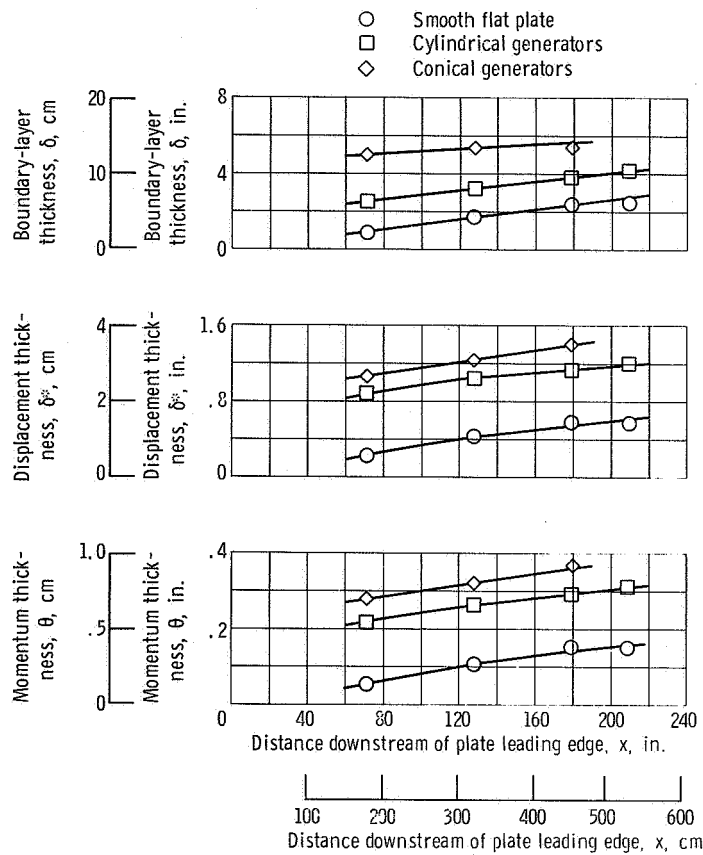


Figure 14. - Comparison of thickness parameters of the three configurations at nominal Mach number of 2.5.

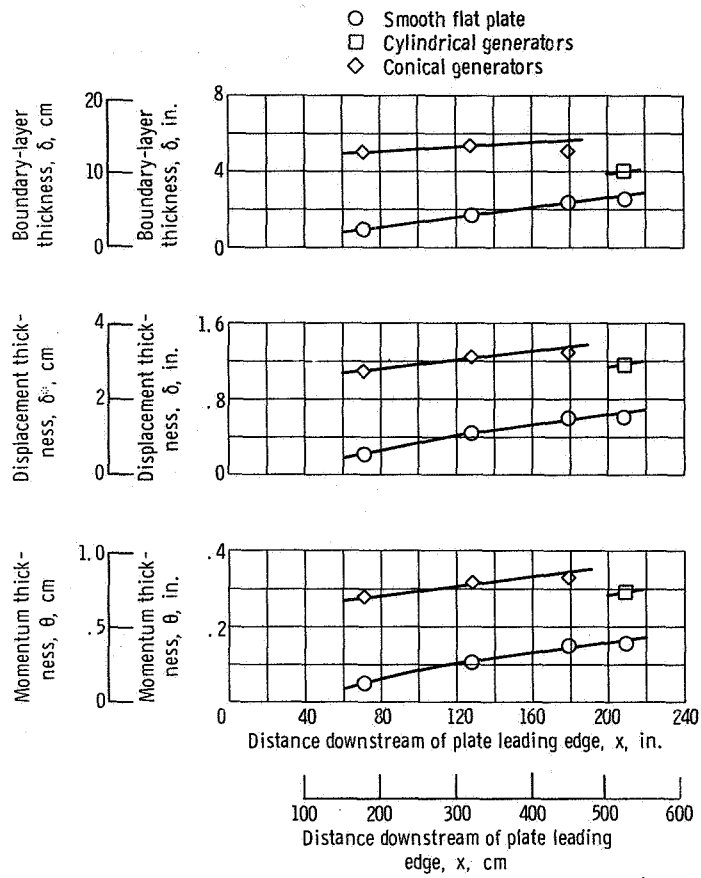


Figure 15. - Comparison of thickness parameters of the three configurations at nominal Mach number, 2.6.

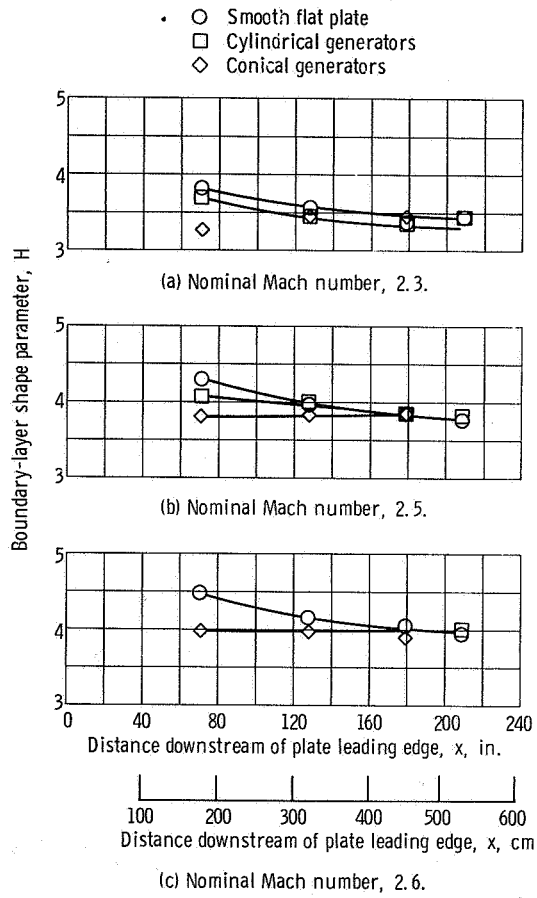


Figure 16. - Comparison of boundary-layer shape parameters.

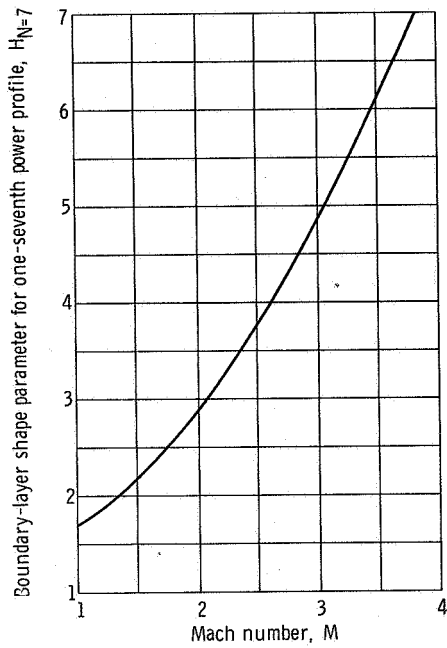


Figure 17. - Effect of Mach number on boundary-layer shape parameter for a one-seventh power velocity profile.

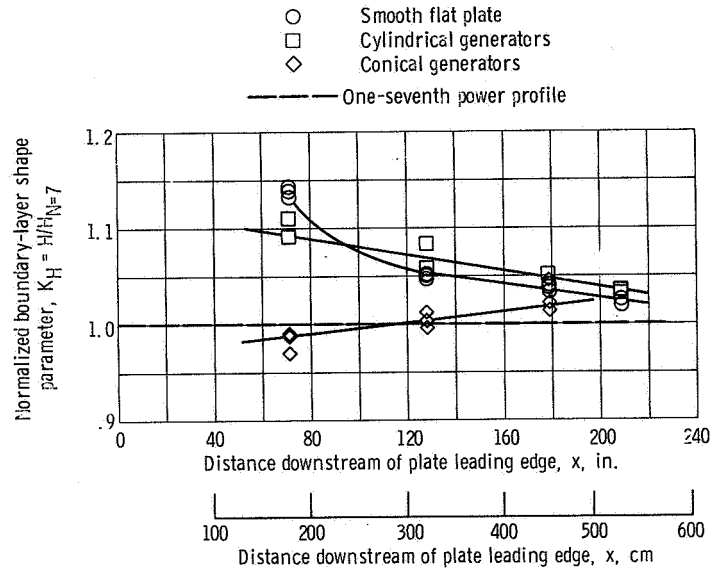


Figure 18. - Comparison of normalized boundary-layer shape parameters.

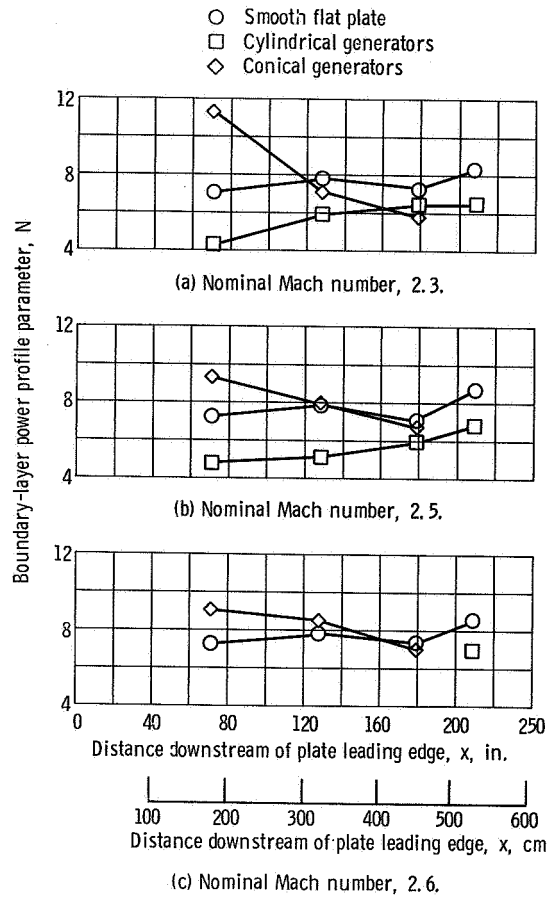


Figure 19. - Comparison of boundary-layer power profile parameters.

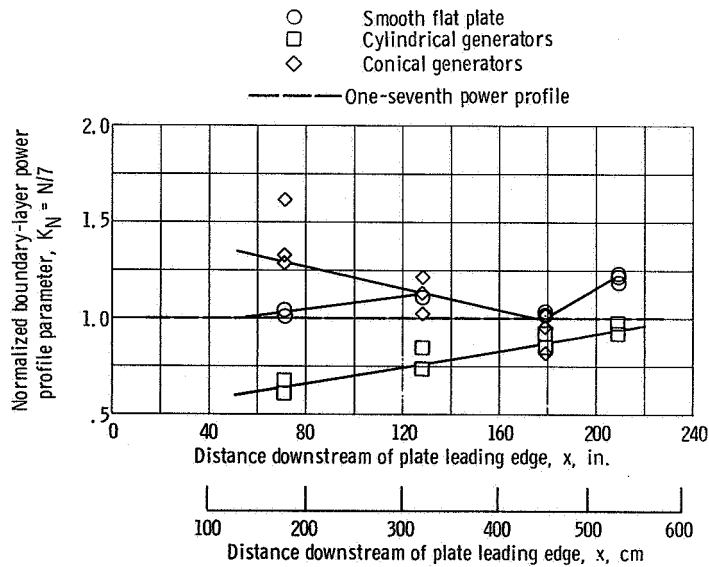


Figure 20. - Comparison of normalized boundary-layer power profile parameter.

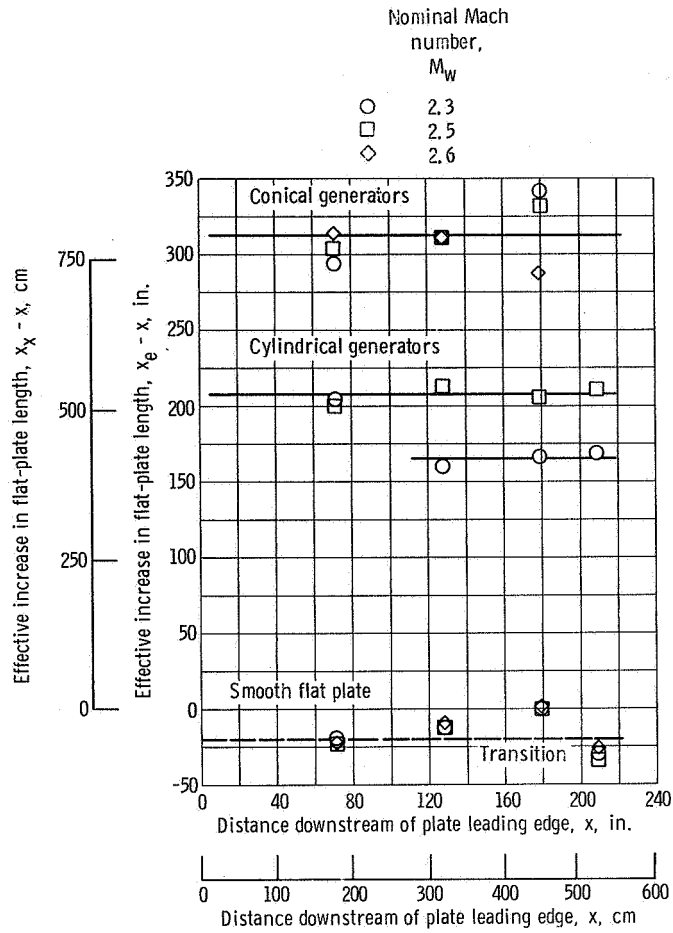


Figure 21. - Effective flat-plate-length calculation.

• Static-pressure instrumentation

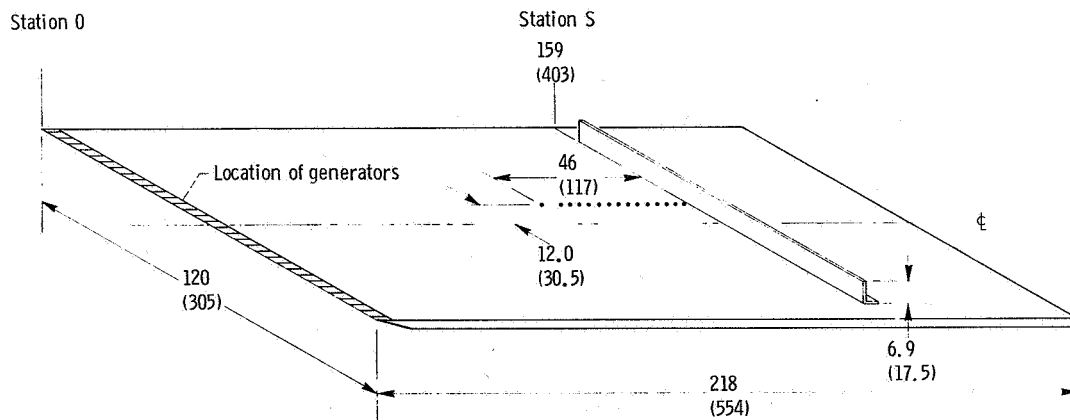
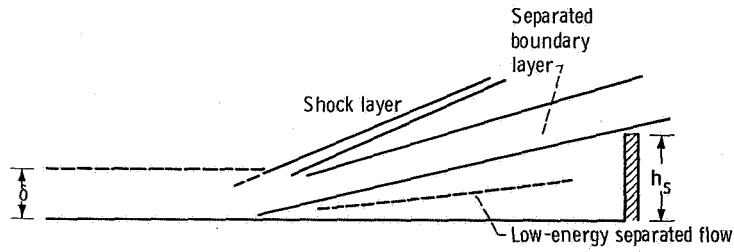
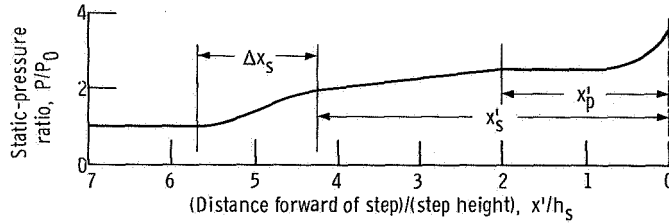


Figure 22. - Installation of forward-facing step and instrumentation on model. (Dimensions are in inches (cm).)



(a) Flow-field profile.



(b) Plate pressure distribution.

Figure 23. - Forward-facing-step flow-field profile and associated plate pressure distribution prediction (ref. 8).

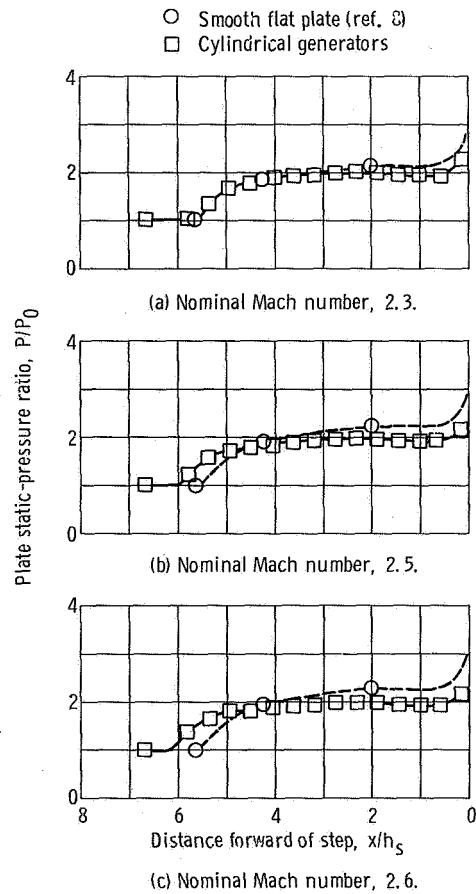


Figure 24. - Surface pressure distribution produced by a boundary-layer separation ahead of a forward-facing step.

NATIONAL AERONAUTICS AND SPACE ADMINISTRATION

WASHINGTON, D. C. 20546

OFFICIAL BUSINESS
PENALTY FOR PRIVATE USE \$300

FIRST CLASS MAIL



POSTAGE AND FEES PAID
NATIONAL AERONAUTICS AND
SPACE ADMINISTRATION

POSTMASTER: If Undeliverable (Section 13
Postal Manual) Do Not Return

"The aeronautical and space activities of the United States shall be conducted so as to contribute . . . to the expansion of human knowledge of phenomena in the atmosphere and space. The Administration shall provide for the widest practicable and appropriate dissemination of information concerning its activities and the results thereof."

— NATIONAL AERONAUTICS AND SPACE ACT OF 1958

NASA SCIENTIFIC AND TECHNICAL PUBLICATIONS

TECHNICAL REPORTS: Scientific and technical information considered important, complete, and a lasting contribution to existing knowledge.

TECHNICAL NOTES: Information less broad in scope but nevertheless of importance as a contribution to existing knowledge.

TECHNICAL MEMORANDUMS: Information receiving limited distribution because of preliminary data, security classification, or other reasons.

CONTRACTOR REPORTS: Scientific and technical information generated under a NASA contract or grant and considered an important contribution to existing knowledge.

TECHNICAL TRANSLATIONS: Information published in a foreign language considered to merit NASA distribution in English.

SPECIAL PUBLICATIONS: Information derived from or of value to NASA activities. Publications include conference proceedings, monographs, data compilations, handbooks, sourcebooks, and special bibliographies.

TECHNOLOGY UTILIZATION PUBLICATIONS: Information on technology used by NASA that may be of particular interest in commercial and other non-aerospace applications. Publications include Tech Briefs, Technology Utilization Reports and Technology Surveys.

Details on the availability of these publications may be obtained from:

SCIENTIFIC AND TECHNICAL INFORMATION OFFICE

NATIONAL AERONAUTICS AND SPACE ADMINISTRATION

Washington, D.C. 20546